



Solar-Wind High-Speed Stream (HSS) Alfvén Wave Fluctuations at High Heliospheric Latitudes: *Ulysses* Observations During Two Solar-Cycle Minima

Ezequiel Echer¹ · Adriane Marques de Souza Franco^{1,2,3} · Edio da Costa Junior⁴ · Rajkumar Hajra⁵ · Mauricio José Alves Bolzan²

Received: 27 April 2022 / Accepted: 5 October 2022
© The Author(s), under exclusive licence to Springer Nature B.V. 2022

Abstract

We study Alfvén wave fluctuations in solar-wind high-speed streams (HSSs) at high heliolatitudes during the last two solar-cycle minima (SCM). Solar-wind plasma and interplanetary magnetic field (IMF) measured by *Ulysses* during four 50-day intervals in 1994, 1995, 2007, and 2008 were analyzed using wavelet and Fourier analyses, cross-correlation and kurtosis techniques. Intervals during 1994 and 1995 (2007 and 2008) correspond to the *Ulysses* polar passes through the southern and northern solar hemispheres, respectively, during the minimum between Cycles 22 and 23 or SCM_{22–23} (the minimum between Cycles 23 and 24 or SCM_{23–24}). The solar-wind plasma density [N_p], IMF magnitude [B_0], and IMF-component variances are found to be lower during SCM_{23–24} than during SCM_{22–23} by $\approx 20\text{--}30\%$. The cross-correlation between the plasma velocity and IMF vector components, an indicative of Alfvénicity, is smaller during SCM_{23–24} than during SCM_{22–23}. The Alfvén wave periodicity exhibits a large range, from ≈ 8 hours to 10 days, with peak occurrences near 1–5 days during both minima. The statistical kurtosis analysis shows that the IMF distributions are mostly sub-Gaussian. Further, the Fourier power law analysis reveals a higher spectral power of transverse IMF components B_t and B_n than the radial field-aligned component B_r . The power spectrum shows a spectral break near 10^{-4} Hz, with its high-frequency portion following a -1.7 power law dependence (Kolmogorov spectrum), while the low-frequency portion shows an ≈ -1.0 power law index dependence. This low-frequency index is slightly higher during SCM_{22–23} (-0.65 to -0.87) than during SCM_{23–24} (-0.49 to -0.78). We conclude that while the Alfvénicity of the high-latitude HSSs does not vary substantially between the two minima, the amplitude of the Alfvén wave fluctuations is reduced during SCM_{23–24} compared to SCM_{22–23}.

✉ E. Echer

¹ National Institute for Space Research (INPE), Sao Jose dos Campos, Brazil

² Federal University of Jataí, Jataí, Brazil

³ Federal University of Southern and Southeastern of Para (UNIFESSPA), Marabá, Brazil

⁴ Federal Institute of Minas Gerais (IFMG) - Campus Formiga, Formiga, Brazil

⁵ Indian Institute of Technology Indore, Simrol, Indore 453552, India

Keywords Coronal holes · Magnetic fields, interplanetary · Solar cycle · Solar wind · Alfvén waves

1. Introduction

The polar regions of the Sun are dominated by coronal holes, which are large-scale unipolar magnetic field regions. These regions have very low plasma density and brightness and thus appear dark in X-rays and other wavelengths (Krieger, Timothy, and Roelof, 1973; Sheeley, Harvey, and Feldman, 1976; Priest, 1995; Cranmer, 2009). The coronal hole magnetic field polarity changes from even to odd solar cycles (Hathaway, 2010). From the coronal holes, high-speed streams (HSSs) are emitted, which are embedded with unidirectional interplanetary magnetic field (IMF) (Krieger, Timothy, and Roelof, 1973; Cranmer, 2009). Large oscillations in HSS IMF components have been identified as Alfvén waves (Alfvén, 1942; Belcher and Davis Jr., 1971; Smith et al., 1995).

For the Alfvén waves, the magnetic field provides the restoring force while ions provide the inertia (Bittencourt, 2010). Further, Alfvén waves are oscillations in solar-wind velocity and IMF components, but not in plasma density or IMF magnitude (Belcher and Davis Jr., 1971; Bittencourt, 2010). The energy propagation and dissipation of Alfvén waves in the solar corona is one of the proposed mechanisms for coronal heating (Priest, 1995; Cranmer, 2009). While Alfvén waves are observed specially in coronal-hole emanated HSSs (Belcher and Davis Jr., 1971; Smith et al., 1995; Tsurutani et al., 1996), their presence in the slower solar-wind has also been reported (e.g. D'Amicis, Matteini, and Bruno, 2019). Furthermore, Alfvén waves are the most frequently observed solar-wind fluctuations. Due to their noncompressive nature, they do not suffer damping and thus last longer and dominate the solar-wind turbulence (Bruno and Carbone, 2013).

Alfvén wave permeated HSSs are characterized by very high plasma speeds, from ≈ 750 to $\approx 800 \text{ km s}^{-1}$, low plasma densities and temperatures, and “open” magnetic field lines, that is, the magnetic field is oriented mainly in the radial direction, away from or toward the Sun. The HSS flow, with frozen-in open magnetic field lines attached to the Sun at one end, expands into the interplanetary space (e.g. Zhang et al., 2003; Cranmer, 2009).

Wang and Sheeley (2006) presented the solar sources of the HSSs observed by the *Ulysses* spacecraft. During a solar cycle, the coronal-hole distribution varies in the solar corona and so does the extension of the HSSs in the heliosphere (Wang and Sheeley, 2006; Schrijver and Liu, 2008). Near solar maximum, coronal holes are confined to polar regions and even disappear. On the other hand, during the declining phase, coronal holes dominate the Sun's polar regions and extend to lower heliographic latitudes (Krieger, Timothy, and Roelof, 1973; Sheeley, Harvey, and Feldman, 1976; Tsurutani et al., 1996; Schwenn, 2006; Cranmer, 2009). With this extension, HSSs can reach the equatorial plane where they can interact with the slow solar wind, leading to the formation of corotating interaction regions (CIRs: Smith and Wolfe, 1976; Tsurutani et al., 1996; Balogh et al., 1999).

The *Ulysses* spacecraft was launched in 1990, near the Solar Cycle 22 maximum, and then moved away from the Sun at low latitudes near the ecliptic plane until encountering Jupiter in early 1992. The gravitational assist put *Ulysses* in a polar orbit around the Sun (Smith et al., 1995). *Ulysses* went first to high southern latitudes, with a maximum latitude of 80.2° S during September 1994, then reached a maximum northern latitude of 80.2° N during July 1995. This first orbit occurred during the declining phase of Solar Cycle 22 and subsequent minimum between Cycles 22 and 23. As a consequence, *Ulysses* observed a simple configuration of slow streams at low latitudes and HSSs at higher latitudes originating from the polar coronal holes (Phillips et al., 1995; McComas et al., 2000). CIRs were

typically observed at mid latitudes (Gosling et al., 1993; Balogh et al., 1999; Neugebauer, 1999).

The *Ulysses* second orbit occurred around the Solar Cycle 23 maximum. In contrast to the simple structure observed during the first orbit, the *Ulysses* second orbit revealed a complex global structure of the 3D solar wind at all heliolatitudes. This complex structure was driven by a complicated mixture of streams arising from multiple sources at the Sun (McComas et al., 2002, 2003), including streamers, coronal mass ejections (CMEs), small coronal holes, and active regions (Neugebauer et al., 2002). The two magnetic-sector structures largely persisted throughout this interval, but the apparent magnetic-dipole axis rotated as the Sun's magnetic polarity reversed with its orientation being nearly perpendicular to the Sun's rotation axis around the solar maximum (Smith et al., 2001).

During *Ulysses'* third orbit, starting in mid-2004, the solar activity was low again, and the latitudinal solar-wind configuration was once again similar to that during the first orbit (Richardson, 2014). However, this third orbit corresponds to an interval near the deep minimum in solar activity between Cycles 23 and 24, during 2008–2009 (Smith and Balogh, 2008; Tsurutani, Echer, and Gonzalez, 2011). The *Ulysses* data acquisition ended in the middle of 2008. For heliolatitudes $> 40^\circ$, it was observed that the solar wind in the third orbit was less dense (−17%) and cooler (−14%), with a smaller dynamic pressure (−22%) than in the first orbit (McComas et al., 2008). This was due to the weaker polar coronal-hole flows in the 2007 minimum (McComas et al., 2008; Ebert et al., 2009). Further, polar coronal-hole solar-wind plasma density and IMF magnitude appeared to fall less sharply with heliocentric distance in the third orbit than in the first one (Ebert et al., 2009).

Smith and Balogh (2008) showed that during the third orbit, the solar open magnetic flux over the Sun's poles decreased by a factor of 0.64, and the total magnetic field variances decreased by a factor of 0.75 from 1993–1995 to 2006–2008. Virtanen and Mursula (2010) reported a modulus of the IMF radial component at high latitudes higher by 0.2 nT in the southern solar hemisphere than in the northern hemisphere during both solar-cycle minima, 1994–1995 and 2007. It was also found (Balogh and Erdős, 2013) that the magnetic fluxes were higher in the southern hemisphere than in the northern hemisphere in both solar minima, and in both hemispheres they were higher during 1994–1997 than during 2006–2008. Finally, during the *Ulysses'* (third orbit) southern passage, a small modulation was observed in the high-latitude galactic cosmic rays, which was attributed to the absence of any large and stable coronal hole in this minimum (Dunzlaff et al., 2008). Indeed, the 2007–2008 solar minimum was characterized by weak polar magnetic fields and smaller polar coronal holes (de Toma, 2012).

The aim of the present work is to perform a detailed study on the HSS Alfvén wave fluctuations from high polar latitudes of the Sun during the last two solar-cycle minima (SCM), 1994–1995 and 2007–2008 (hereafter referred as SCM_{22–23} and SCM_{23–24}, respectively) using *Ulysses* observations. We will explore the comparative features of the Alfvén wave turbulence using wavelet, Fourier, cross-correlation, and kurtosis analysis techniques during these two solar minima. While there have been several works studying the high-latitude solar-wind Alfvén waves (e.g. Smith et al., 1995; Tsurutani et al., 1996), those studies mainly focused on SCM_{22–23}. A comparative study of Alfvén waves during both solar minima has not been reported to our knowledge. We will conduct this comparative study to determine the differences, if any, in HSS turbulence between the two solar minima.

Table 1 Hourly solar-wind plasma and IMF data availability for each polar pass of 1200 hours^a.

	Interval 1 Days 245–294 of 1994	Interval 2 Days 212–261 of 1995	Interval 3 Days 043–092 of 2007	Interval 4 Days 006–055 of 2008
Plasma data	1176 (98.0%)	1186 (98.8%)	1196 (99.7%)	866 (72.2%)
IMF data	1191 (99.3%)	1186 (98.8%)	1200 (100%)	1163 (96.9%)

^aNumbers between parentheses represent percentages of total 1200 observation hours.

2. Database and Analysis Methods

2.1. Ulysses Data and Selection of the Studied Intervals

We analyze the 1-minute, 1-hour, and 1-day averaged solar-wind plasma parameters, namely speed [V_{sw}], density [N_p], temperature [T_p], and the IMF components measured by *Ulysses*. The data were collected from NASA COHOWeb (omniweb.gsfc.nasa.gov/coho/). The 1-day data are used to show an overview of the solar-wind conditions during the full *Ulysses* mission. The 1-hour data are used to characterize average solar-wind conditions and compute the correlation between magnetic field and velocity vector components during the selected polar passes. The 1-minute magnetic field data are used to study the solar-wind turbulence. The *Ulysses* magnetometer consisted of two sensors, a *Vector Helium Magnetometer* (VHM) and a *FluxGate Magnetometer* (FGM). The two magnetometer sensors were located on the radial boom of the *Ulysses* spacecraft: the VHM sensor at the end of a 5 m boom, the FGM sensor at a 1.2 m boom inboard from the VHM. The FGM sensor consisted of three identical single-axis ring-core fluxgate sensors arranged in an orthogonal triad (Balogh et al., 1992). Plasma data were obtained from the *Solar Wind Observations Over the Poles of the Sun* (SWOOPS) experiment, which used two electrostatic analyzers for positive ions and electrons. The SWOOPS ion analyzer measured 3D velocity space distributions of positive ions. In its normal solar wind mode, the instrumental energy range was from 0.25 to 12 keV/q (Bame et al., 1992).

The spacecraft-centered radial–tangential–normal (RTN) coordinate system is used in this study. In the RTN system, R is directed along the Sun-to-spacecraft unit vector [$\hat{\mathbf{r}}$], T is defined as $\Omega \times \hat{\mathbf{r}} / |\Omega \times \hat{\mathbf{r}}|$, Ω is directed along the Sun’s rotation axis, and N completes the right-handed coordinate system.

Figure 1 shows an overview of the solar-wind plasma and IMF observations by *Ulysses* during the entire mission period. One-day averaged data are used to highlight the intervals of analyses. From top to bottom, the panels are the sunspot number [R_z], the solar-wind plasma [V_{sw}], N_p , the IMF magnitude [B_0], and the *Ulysses* heliocentric distance and heliolatitude, respectively. The high-latitude polar passes during the two solar-cycle minima are marked with dotted lines and downward arrows in the top panel. Four intervals selected for detailed analyses are listed in Table 1. They correspond to the *Ulysses* polar passes (heliolatitudes $> 70^\circ$) during the solar minimum periods (SCM_{22–23} and SCM_{23–24}): 1994 and 1995, and 2007 and 2008, respectively. The heliocentric distance ranging from 2.0 to 2.4 AU was selected to reduce the radial dependence of the solar-wind parameters.

Eliminated from this data set are all interplanetary CME (ICME) intervals, the cometary encounters, and the Jupiter magnetospheric flyby interval. The ICME intervals are taken from Richardson (2014). The Jupiter flyby in 1992 is determined from Smith, Wenzel, and Page (1992) and Balogh et al. (1992). Ten days around each of the following cometary

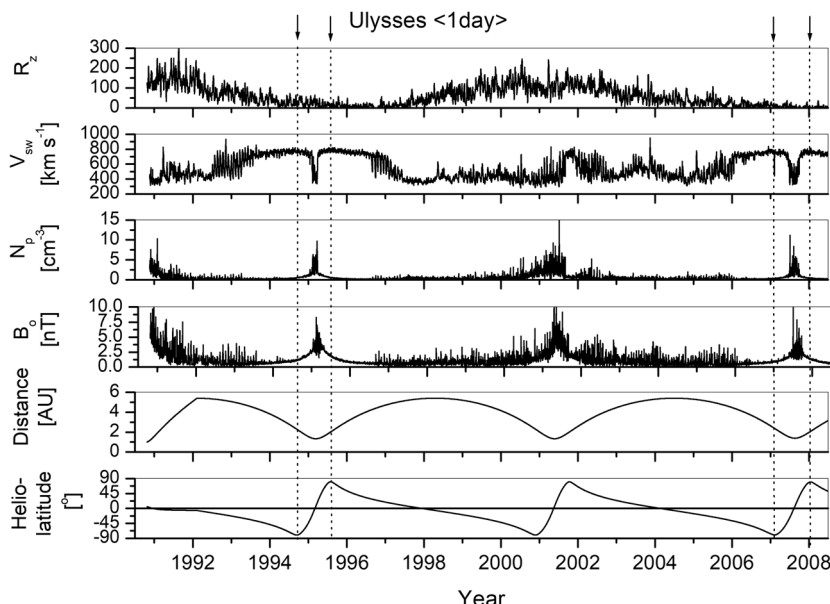


Figure 1 Overview of the *Ulysses* mission. From top to bottom, panels are the 1-day averaged sunspot number [R_z], solar-wind plasma velocity [V_{sw}], proton density [N_p], IMF magnitude [B_0], the heliocentric distance, and heliolatitude of the *Ulysses* spacecraft, respectively. The downward arrows at the top and the dotted lines show the selected intervals for this study (see Table 1 for details).

encounters were removed: Comet Hyakutake C/1996 B2 on 1 May 1996 (Jones, Balogh, and Horbury, 2000), Comet McNaught-Hartley C/ 1999 T1, and possibly comet C/2000 S5 (SOHO) on 19 October 2000 (Gloeckler et al., 2004), and comet McNaught C/2006 P1 on 3–4 February 2007 (Neugebauer et al., 2007).

Availability of the solar-wind plasma and IMF data during the intervals are listed in Table 1 based on the above criteria. There were several plasma data gaps in 2008 (*Ulysses'* last year of operation). The IMF data are available for > 96% of the time for all intervals. Plasma data availability is > 98% of the time for the first three intervals, but only for $\approx 72\%$ of the time during the Interval 4.

2.2. Methods

Wavelet analysis is performed to identify main periodicities in the solar wind and characterize the main scales of Alfvén wave fluctuations. The wavelet transform (WT) is a suitable technique to analyze non-stationary time series. It decomposes a signal in translated and scaled (dilated or compressed) versions of the mother wavelet, each one multiplied by an appropriate coefficient (Torrence and Compo, 1998). The Morlet wavelet is one example of continuous WT that can be used to study periodic signals and is the wavelet mother chosen for this study (Torrence and Compo, 1998; Franco et al., 2020).

The correlation analysis (Davis, 2002) between the IMF- and the plasma velocity-components is performed to study the HSS Alfvénicity. Similar methods have been used in earlier works (e.g. Belcher, Davis Jr., and Smith, 1969; Belcher and Davis Jr., 1971; Smith et al., 1995).

We computed the variance of the IMF components (in nT²) for each interval (Davis, 2002). It gives an indication of the degree of the IMF variability.

Kurtosis is computed to study the HSS turbulence. It can identify intermittence by computing the variable probability density function (PDF) and estimating its deviation from a Gaussian distribution. When a distribution has a high-energy tail, with strong deviations from a Gaussian distribution, a higher occurrence frequency of intermittent events is indicated, which can be an additional source of waves and instabilities (Bolzan and Echer, 2014). Kurtosis is a measure of the sharpness of a distribution. Gaussian distributions have kurtosis values close to 3, while sub-Gaussian ones have kurtosis less than 3. Distributions with kurtosis values greater than 3 tend to have heavy tails, or outliers (Davis, 2002; Franco et al., 2022).

The Fourier spectrum of a time series is fitted by a power-law function as: $P = cf^\alpha$, where P is the Fourier spectral power, c is a constant, f is the frequency, and α is the power-law index (Bracewell, 2014). This is widely used in turbulence studies to characterize the plasma wave activity domains as well as the turbulent activity dependence on the system scales or frequencies of oscillations in the system (Bolzan and Echer, 2014).

3. Results

3.1. Overview and General Statistics

Figure 2 shows the solar-wind observations during the four selected intervals. For each of these intervals, the panels show one-hour average of solar-wind plasma V_{sw} , N_p , T_p , and IMF B_0 , respectively. Ranges of heliocentric distance and heliolatitude, statistical averages (along with standard deviations) and median values of the solar wind plasma parameters, plasma- β , IMF components and B_0 , Alfvén velocity [V_A], and IMF variances during the intervals are listed in Table 2. β is defined as the ratio of the plasma pressure to the magnetic pressure. V_A is estimated as $B_0/\sqrt{\mu_0\rho}$, where μ_0 is the free space permeability, and ρ is the solar-wind mass density.

During the four selected intervals, V_{sw} is $> 700 \text{ km s}^{-1}$, and IMF B_0 is $\approx 1.5 \text{ nT}$, with relatively small variability. N_p and T_p are also relatively stable during the intervals (Figure 2, Table 2).

It is noted that N_p and B_0 are smaller during SCM_{23–24} (2007 and 2008) than during SCM_{22–23} (1994 and 1995) by factors of $\approx 20–30\%$. P_{sw} in the southern (northern) hemisphere is ≈ 1.7 (≈ 1.3) times higher during SCM_{22–23} than during SCM_{23–24} (Table 2). These results agree with previous studies reporting weakening of the solar activity during Cycle 24 compared to Cycle 23 based on the *Ulysses* observations (e.g. McComas et al., 2008), and solar-wind observations at 1 AU (e.g. Tsurutani, Echer, and Gonzalez, 2011; Franco et al., 2021; Hajra et al., 2021; Hajra, 2021).

The plasma- β values vary between ≈ 1.6 and ≈ 2.0 , indicating plasma pressure up to 2 times of the magnetic pressure over the solar poles. In addition, higher β values in SCM_{23–24} than in SCM_{22–23} imply that the magnetic pressure had a higher decrease than the plasma pressure from SCM_{22–23} to SCM_{23–24}.

V_A is slightly smaller during SCM_{23–24} ($\approx 39–40 \text{ km s}^{-1}$) than during SCM_{22–23} ($\approx 43–44 \text{ km s}^{-1}$). This is a reduction of $\approx 10\%$, which can be attributed to the smaller B_0 during Cycle 24 compensating the smaller N_p also seen during this cycle.

The IMF values and variances are higher during SCM_{22–23} than during SCM_{23–24}. Further, the IMF-component variances are much higher than the IMF-magnitude variances. In

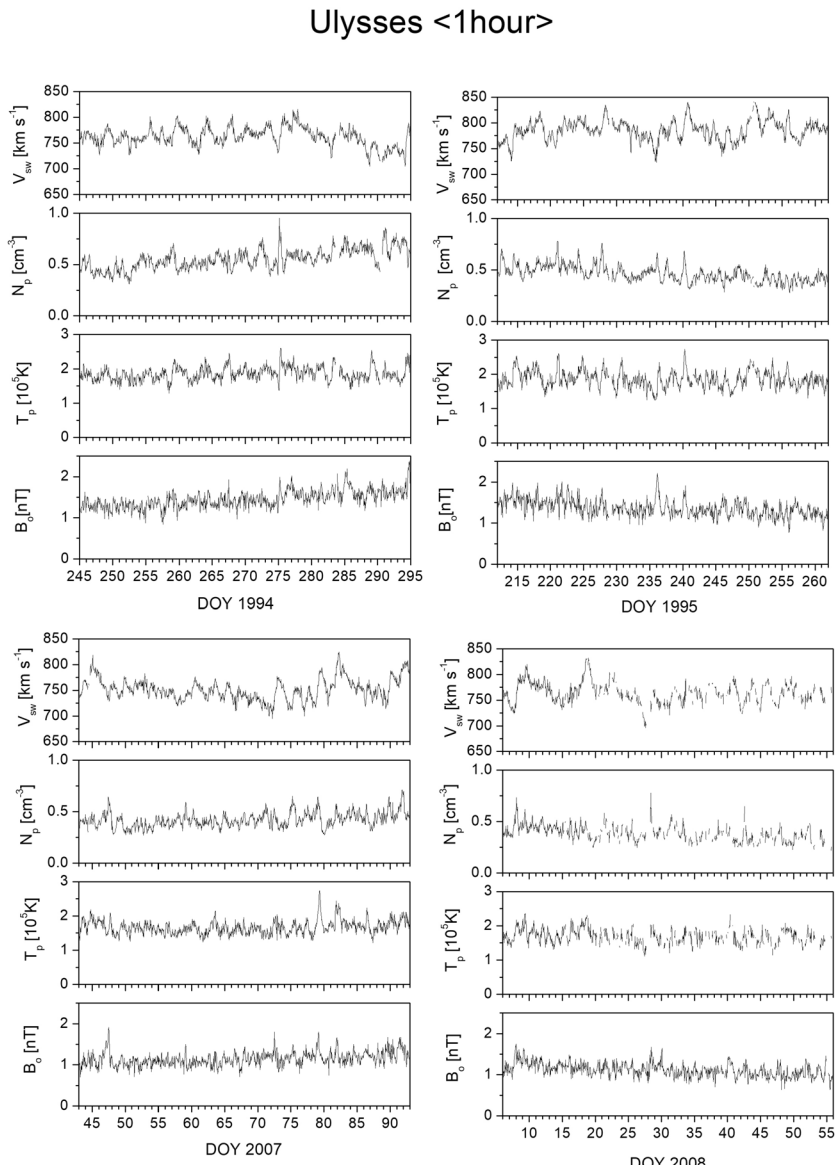


Figure 2 The *Ulysses* solar-wind observations during the four intervals (1994, 1995, 2007, and 2008) used in this study. For each of the intervals, panels show the 1-hour averaged solar-wind plasma V_{sw} , N_p , T_p , and IMF B_0 , respectively.

addition, the B_t and B_n variances are more than twice higher than the B_r variances during any interval. Most of the IMF is directed along the radial direction (B_r -component); therefore, the variance is much higher in the transverse direction (perpendicular to the field) than in the parallel direction. It agrees with Alfvén waves, which are known to show large transverse fluctuations and smaller variation along the field direction.

Table 2 Statistics of the HSS solar-wind plasma and the IMF parameters during the four selected *Ulysses* polar passes.

Parameter	Interval 1	Interval 2	Interval 3	Interval 4
Distance ^a [AU]	[2.02; 2.37]	[2.01; 2.31]	[2.01; 2.35]	[2.01; 2.35]
Heliolatitude ^a [deg]	[−80.2; −74.5]	[72.1; 80.2]	[−79.7; −70.7]	[74.0; 79.7]
$\langle V_{sw} \rangle^b$ [km s ^{−1}]	762.2 ± 18.4 (762.9)	785.5 ± 19.4 (786.6)	751.1 ± 21.0 (749.8)	764.5 ± 20.6 (764)
$\langle N_p \rangle^b$ [cm ^{−3}]	0.55 ± 0.10 (0.55)	0.46 ± 0.08 (0.45)	0.42 ± 0.07 (0.41)	0.39 ± 0.08 (0.39)
$\langle T_p \rangle^b$ [10 ⁵ K]	1.86 ± 0.2 (1.84)	1.86 ± 0.24 (1.84)	1.67 ± 0.2 (1.65)	1.70 ± 0.22 (1.69)
$\langle B_0 \rangle^b$ [nT]	1.45 ± 0.21 (1.44)	1.37 ± 0.2 (1.35)	1.15 ± 0.17 (1.13)	1.12 ± 0.16 (1.11)
$\langle P_{sw} \rangle^b$ [nPa]	0.53 ± 0.09 (0.53)	0.48 ± 0.08 (0.47)	0.31 ± 0.07 (0.30)	0.38 ± 0.08 (0.37)
$\langle \beta \rangle^b$	1.76 ± 0.52 (1.68)	1.67 ± 0.54 (1.57)	2.07 ± 0.69 (1.94)	1.86 ± 0.6 (1.76)
$\langle B_r \rangle^b$ [nT]	−0.64 ± 0.38 (−0.66)	0.57 ± 0.39 (0.59)	0.48 ± 0.33 (0.5)	−0.43 ± 0.33 (−0.46)
$\langle B_t \rangle^b$ [nT]	0.10 ± 0.66 (0.14)	−0.11 ± 0.64 (−0.12)	−0.013 ± 0.52 (−0.03)	0.011 ± 0.49 (0.02)
$\langle B_n \rangle^b$ [nT]	0.058 ± 0.64 (0.06)	0.044 ± 0.61 (0.03)	−0.021 ± 0.51 (−0.03)	0.02 ± 0.53 (0.05)
$\sigma_{B_0}^2$ [nT ²]	0.044	0.041	0.029	0.027
$\sigma_{B_r}^2$ [nT ²]	0.14	0.15	0.11	0.11
$\sigma_{B_t}^2$ [nT ²]	0.44	0.41	0.27	0.24
$\sigma_{B_n}^2$ [nT ²]	0.41	0.37	0.26	0.28
$\langle V_A \rangle$ [km s ^{−1}]	42.8 ± 5.2 (42.4)	44.1 ± 5.5 (43.9)	38.8 ± 4.9 (38.6)	39.8 ± 4.7 (39.9)

^aRange.^bMean ± standard deviation (median).

During both solar minima, N_p and B_0 are found to be slightly smaller in the northern hemisphere (Intervals 2 and 4) than in the southern hemisphere (Intervals 1 and 3). The southern-to-northern hemispheric B_0 ratios are 1.06 and 1.03 during SCM_{22–23} and SCM_{23–24}, respectively. The N_p ratios are 1.20 and 1.08, respectively. However, the ratios are very small and may be within the statistical uncertainty, especially for B_0 . The hemispheric asymmetry was also studied by Virtanen and Mursula (2010) and Balogh and Erdős (2013), who found that the field component modulus and flux densities are higher in the southern hemisphere this fact agrees with the present results (Table 2). Further, V_A is also noted to be higher by a smaller amount ($\approx 3\%$) for the northern hemisphere than for the southern hemisphere in both cycles. However, this difference is smaller than the observed variation between the two cycles ($\approx 10\%$).

3.2. Correlation Analysis of Alfvénicity

Figure 3 shows the variations of 1 hour-average IMF- and plasma velocity-components during the four selected intervals. While B_0 and V_{sw} exhibit quasi-steady variations (Figure 2), their components exhibit large fluctuations. The B_r component, which corresponds to the direction where most of the total field is directed, is found to have negative and positive polarities depending on the solar hemisphere and solar cycle. This is consistent with the Sun's magnetic-field polarity reversal at the solar maximum (Hathaway, 2010). During SCM_{22–23}, B_r is negative in the southern hemisphere (1994) and positive in the northern hemisphere (1995). On the other hand, during SCM_{23–24}, B_r is positive in the southern hemisphere (2007) and negative in the northern hemisphere (2008).

While plasma velocity- and IMF-components exhibit high-frequency fluctuations, they seem to be correlated with each other in each panel of Figure 3. This can be an indication

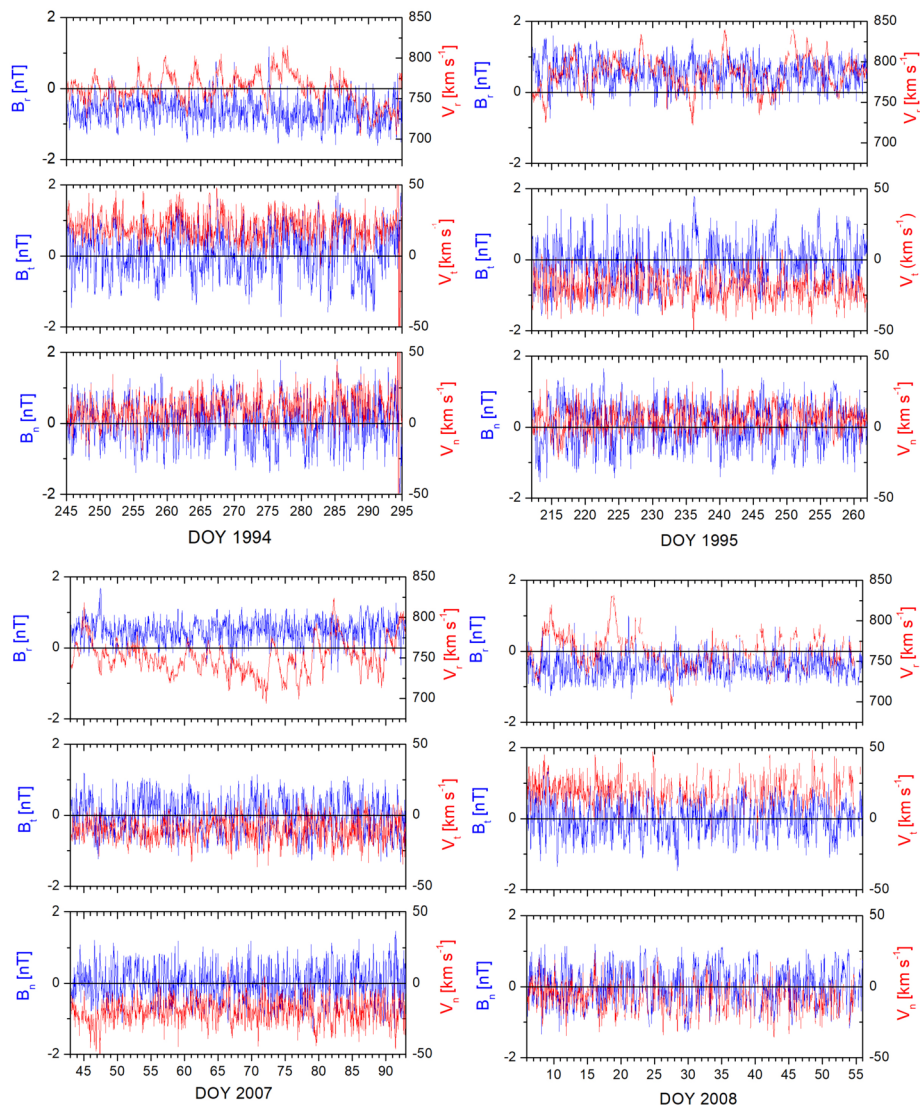


Figure 3 Comparison between the 1 hour-average plasma velocity V_r , V_t and V_n components (red lines, scale on the right) and the IMF B_r , B_t and B_n components (blue lines, scale on the left) components during the four intervals (1994, 1995, 2007, and 2008) under this study.

of Alfvénicity of the selected HSS events. The velocity- and IMF-vector components are in phase during Intervals 1 and 4, while they are 180° out of phase during Intervals 2 and 3.

Figure 4 shows the regression analysis between the 1-hour average plasma velocity- and IMF-components. The linear regression lines and correlation coefficients [r] are shown in each panel. The r -values are also listed in Table 3.

To identify a possible contribution of the data resolution in the Alfvénicity, a correlation analysis is performed between the plasma velocity- and IMF-components at longer time scales, namely 3, 5, 10, and 20 hours. The resultant correlation coefficients [r] are listed

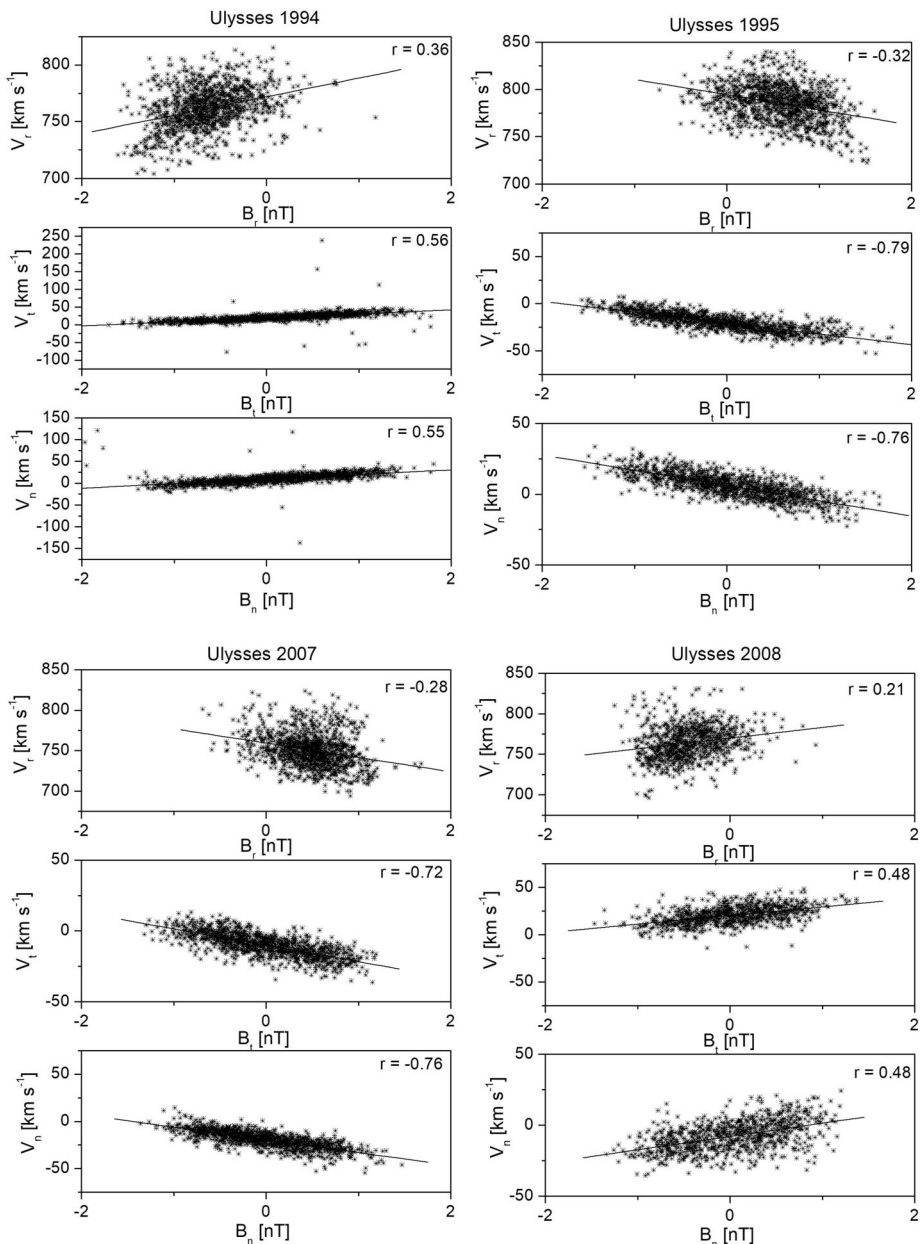


Figure 4 Variations of the 1 hour-average plasma velocity-components with the IMF-components during the four intervals (1994, 1995, 2007, and 2008) under this study. Linear regression lines and correlation coefficients [r] are shown in each panel.

in Table 3 along with the 1 hour correlation results. It can be clearly seen that the r -values are much higher for the T- and N-components than for the R-component for longer scales.

Table 3 Correlation coefficients [r] between the plasma velocity- and the IMF-components during the four intervals.

	Interval 1	Interval 2	Interval 3	Interval 4
Data resolution: 1 hour				
$B_r - V_r$	0.36	-0.32	-0.28	0.21
$B_t - V_t$	0.56	-0.79	-0.72	0.48
$B_n - V_n$	0.55	-0.76	-0.76	0.48
Data resolution: 3 hours				
$B_r - V_r$	0.30	-0.30	-0.23	0.16
$B_t - V_t$	0.62	-0.79	-0.70	0.52
$B_n - V_n$	0.45	-0.73	-0.71	0.47
Data resolution: 5 hours				
$B_r - V_r$	0.28	-0.32	-0.22	0.18
$B_t - V_t$	0.74	-0.78	-0.68	0.47
$B_n - V_n$	0.59	-0.77	-0.72	0.47
Data resolution: 10 hours				
$B_r - V_r$	0.44	-0.38	-0.31	0.29
$B_t - V_t$	0.78	-0.77	-0.72	0.45
$B_n - V_n$	0.73	-0.79	-0.69	0.53
Data resolution: 20 hours				
$B_r - V_r$	0.49	-0.37	-0.35	0.31
$B_t - V_t$	0.74	-0.72	-0.84	0.57
$B_n - V_n$	0.81	-0.69	-0.71	0.53

However, r -values do not change much with the increase in time scales, except for the 1- and 20-hour timescales for the R-component.

During any interval, the correlation coefficient [r] is found to be higher for the T- and N-components than for the R-component. This is expected for the Alfvén wave intervals, which have larger oscillations in the transverse directions compared to the radial direction.

The (positive) correlations during Intervals 1 and 4 and the (negative) anti-correlations during Intervals 2 and 3 (Figure 4, Table 3) are related to the Sun's magnetic-field polarity changes. The Sun's magnetic polarity in each hemisphere is different because of its polarity inversion at the solar maximum. The correlation is positive during periods of negative IMF polarity when the IMF is directed toward the Sun ($B_r < 0$), and the correlation is negative during periods of positive IMF polarity when the IMF is directed away from the Sun ($B_r > 0$) (Belcher, Davis Jr., and Smith, 1969). It is consistent with Alfvén waves propagation outward from the Sun (Belcher, Davis Jr., and Smith, 1969; Smith et al., 1995).

The correlation coefficients are slightly higher during SCM_{22–23} (Intervals 1 and 2) than during SCM_{23–24} (Intervals 3 and 4). The lower correlation in the recent deep minimum could indicate a reduced Alfvénic activity and/or turbulence because of weakening of the Sun's magnetic field (Tsurutani, Echer, and Gonzalez, 2011). High-latitude coronal holes were also smaller and had weaker magnetic fields during this interval (de Toma, 2012), which could have implications for the solar-wind Alfvénic turbulence activity.

Although there are other approaches to determine the solar-wind Alfvénicity, such as the computation of Elsasser variables (Bruno and Carbone, 2013), in this work, we used two criteria: 1) pure HSS intervals, free from CIRs, ICMEs and their shocks are selected and 2) the correlation coefficients between the solar-wind velocity and IMF vectors are estimated. The first criterion is owing to the predominance of Alfvénicity in the coronal hole-emanated

HSSs. The second criterion has been used to quantify the degree of Alfvénic fluctuation in several previous works (e.g. Belcher and Davis Jr., 1971; Tsurutani et al., 1996).

3.3. Wavelet Analysis

To identify the major periodicities in the HSS Alfvén waves, we performed wavelet analysis of the (1 minute-average) IMF components during the four intervals. Figures 5, 6, and 7 show the wavelet spectrum for the IMF B_r -, B_t - and B_n -components, respectively. The panels show the temporal variations of the components along with their wavelet spectrum and the global wavelet spectrum (GWS), which is the integrated power over the full interval for each frequency. The wavelet spectral power results of each identified period in the three IMF-components during the four selected intervals are summarized in Figure 8.

All the IMF-components exhibit a large range of periodicity, from a few hours to ≈ 8 days. The wavelet integrated spectral power (energy) is higher for periods of $\approx 2-3$ days and $5-7$ days. The periods shorter than ≈ 1 day are intermittent. The periods of $\approx 1.5-3$ days are quasi-continuous. Overall, the periods longer than 1.5 days seem to have a more continuous distribution and with higher wavelet spectral power for the transverse components. For these components, it seems that the $1.5-7$ day periods present more continuous behavior and with higher wavelet spectral power during SCM₂₂₋₂₃ than during SCM₂₃₋₂₄.

To better visualize the results obtained from the wavelet analysis (Figures 5, 6, and 7), a summary of major periods and their amplitudes is shown in Figure 8. Panels on the left show the main periods for the B_r -component, the middle panels for the B_t -component, and the right panels for the B_n -component. From top to bottom, the panels correspond to the years 1994, 1995, 2007, and 2008, respectively. It can be clearly seen that the periods of a few hours to 8 days have higher amplitude for the B_t - and B_n -components than for the B_r -component.

Higher wavelet spectral power values are seen for the B_t -component in 1994 for periods from 1 to 2.5 and 6.5 days. In 1995, the higher wavelet power is observed for periods of 1, 2, and 3 days. For the B_n -component the higher spectral power is noted around 3 and 7.5 days in 1994 and around 3.5 and 5.5 days in 1995. The corresponding periods for those components in 2007 and 2008 have much smaller wavelet spectral power. Further, the periods for the B_r component have lower wavelet power compared to the transversal IMF components. There are many periods shorter than 3 days with comparable wavelet power. For the very long periods, higher than 10 days, it can be seen that they are isolated periods with low or moderate wavelet power. Further, they are identified only in the B_r -component. This owing to the fact that this interval is close to the limit of the wavelet cone of influence, and that those periods are not considered significant in the analysis.

3.4. Turbulence Analysis

Figure 9 shows the computed kurtosis parameters for the IMF-components and magnitude during the four selected *Ulysses* polar passes using 1-minute resolution data. For all intervals, the kurtosis values of the B_t - and B_n -components are < 3 , indicating a sub-Gaussian behavior. On the other hand, the B_r kurtosis values are mostly found near or slightly above 3. An exception is seen in the 1995 interval, where its kurtosis shows values slightly below 3, especially for the 3 and 15 day scales. B_0 closely follows the B_r behavior but with values higher than 3. This result is expected, since most of the IMF is oriented in the radial direction. However, it is difficult to identify any clear trend for the scales from 1 to 15 days.

However, kurtosis values were found below 3, i.e., sub-Gaussian behavior in a previous work (Echer and Bolzan, 2016) on the study of plasma turbulence in the solar wind near

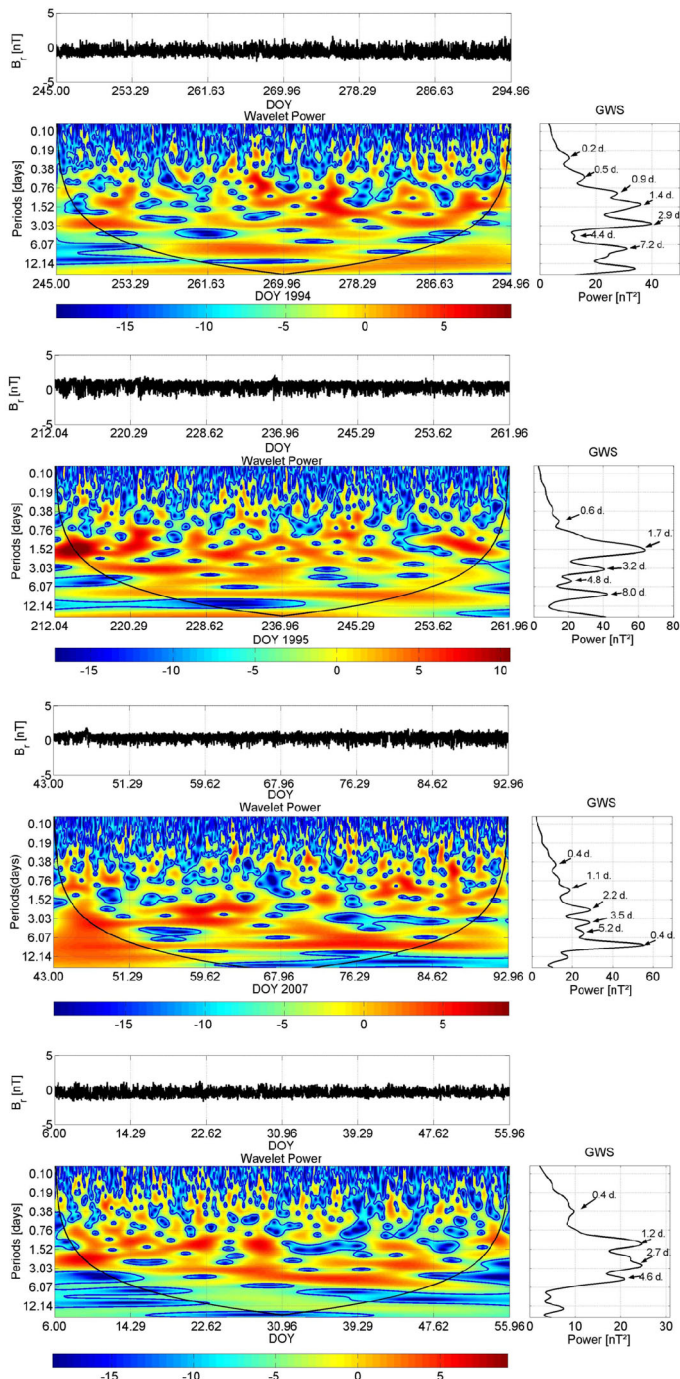


Figure 5 Wavelet analysis of the 1 minute-average IMF B_r during the four intervals (1994, 1995, 2007, and 2008) in this study. For each interval, the top panel shows the temporal variation of B_r , the bottom left panel shows the wavelet spectrum with amplitudes (in arbitrary units) shown by a color bar at the bottom, and the bottom right panel shows the global wavelet spectrum with the major periods marked.

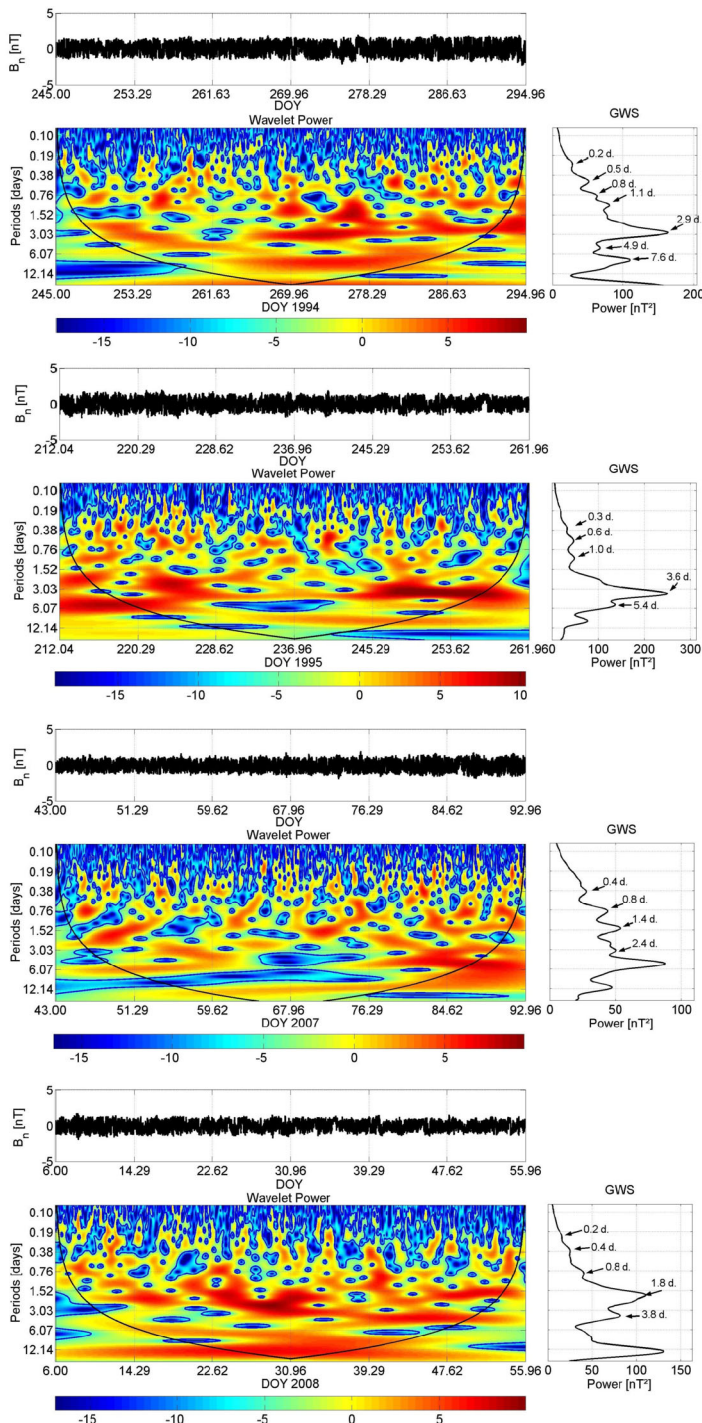


Figure 6 Wavelet analysis of the 1 minute-average IMF B_t during the four intervals (1994, 1995, 2007, and 2008) in this study. Panels are in the same format as in Figure 5.

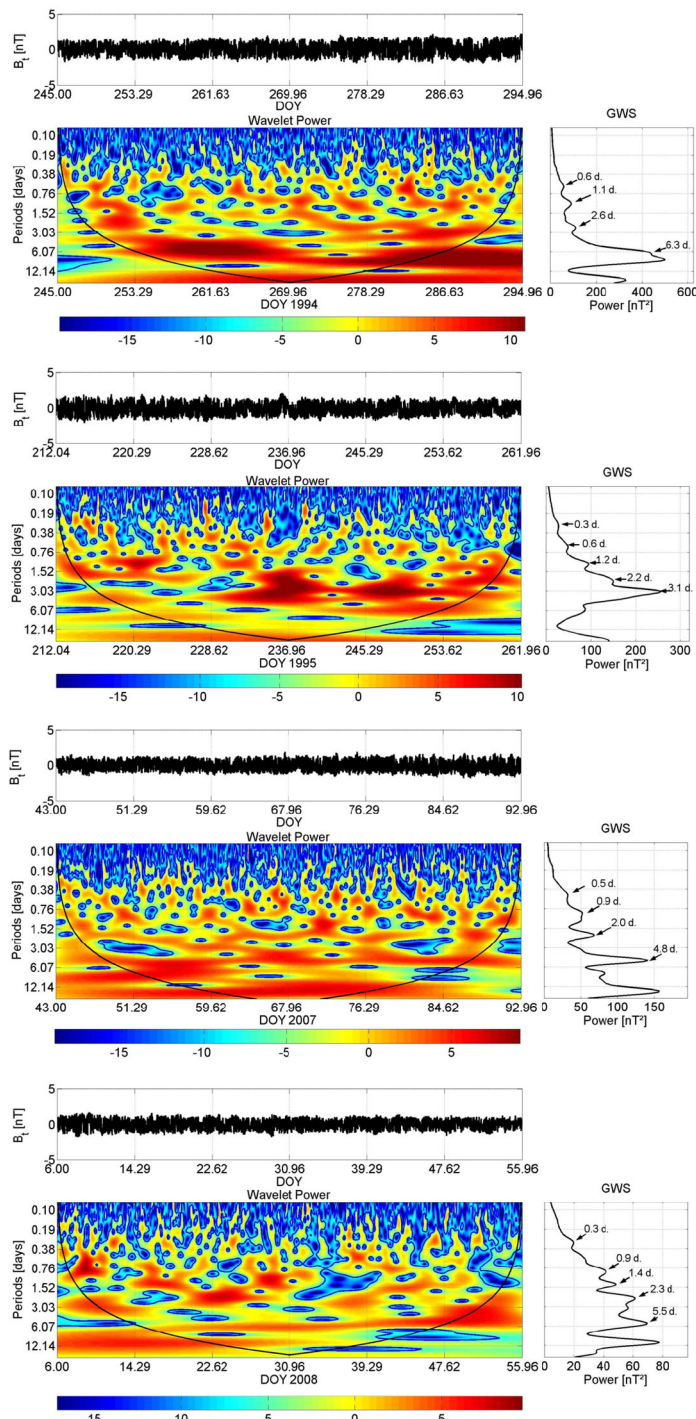


Figure 7 Wavelet analysis of the 1 minute-average IMF B_n during the four intervals (1994, 1995, 2007, and 2008) in this study. Panels are in the same format as in Figure 5.

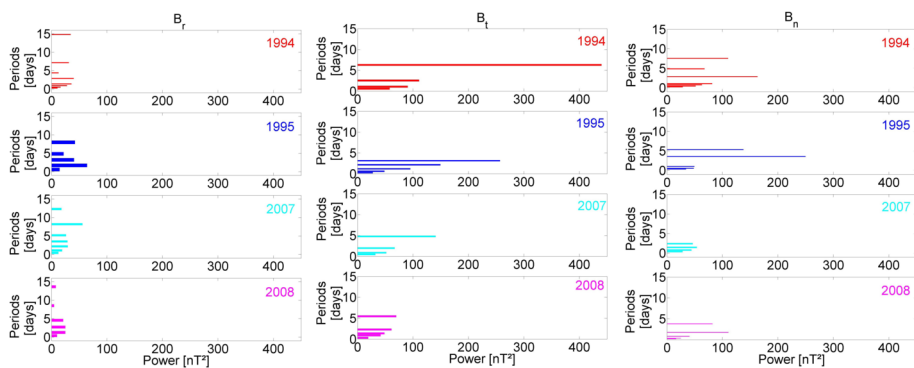


Figure 8 Histogram of identified periods and their wavelet spectral power for the IMF-components. Different intervals are shown by different colors: red for 1994, blue for 1995, cyan for 2007, and magenta for 2008.

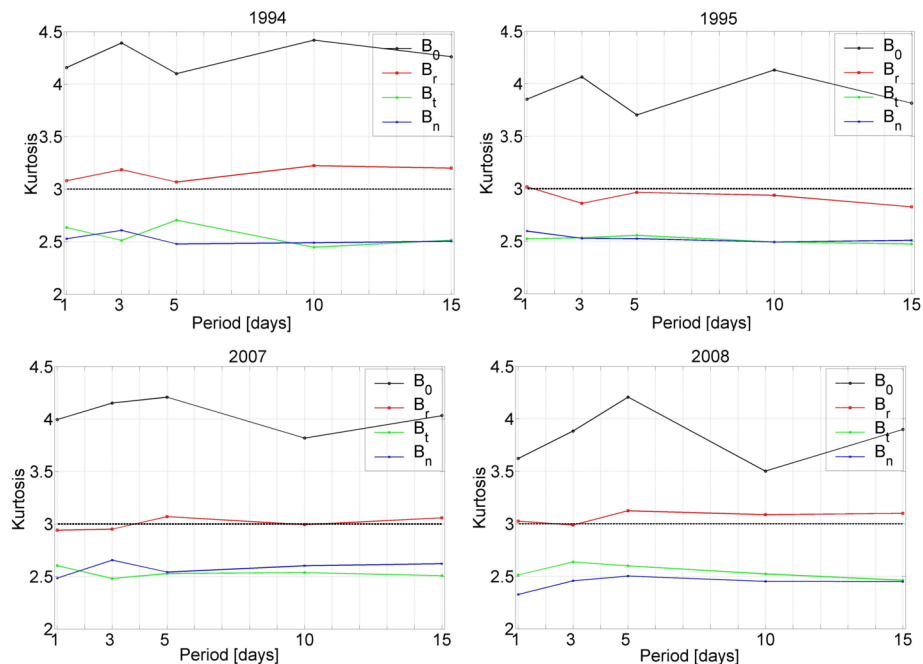


Figure 9 Kurtosis values for the 1 minute-average IMF during the four selected polar crossings (1994, 1995, 2007, and 2008). Colors are black for B_0 , red for B_r , green for B_t , and blue for B_n .

Uranus orbit. According to that work, the sub-Gaussian characteristic may be associated to quasi-periodic waves. This hypothesis was also discussed earlier by Jimenez (1998).

Figure 10 shows the fast Fourier transform (FFT) power spectral density (PSD) and the corresponding power law fitting of the IMF-components during the selected four polar passes. A spectral break near 10^{-4} Hz can be clearly seen in all spectra. Thus, we fitted the high-frequency and low-frequency ranges with two different power law index functions. The spectral break is clearly seen as a “knee” separating the inertial subrange, high-frequency

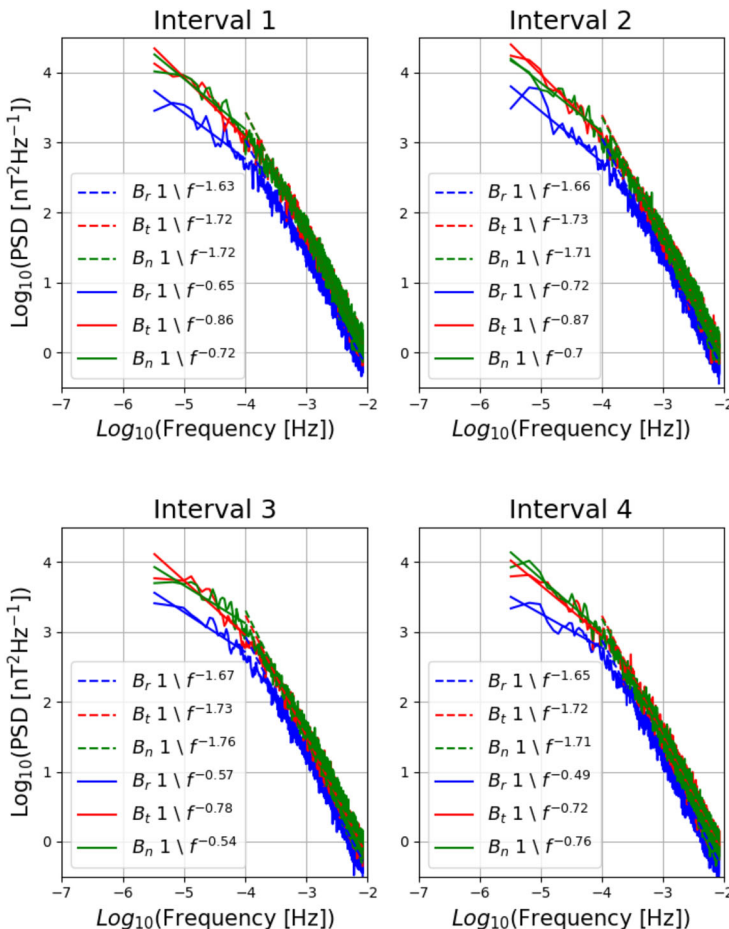


Figure 10 Power spectrum of the IMF-components for the four *Ulysses* polar passes (1994, 1995, 2007, and 2008). The y-axes show the power spectral density (PSD in log scale), and the x-axes show the frequency (log scale). Power law fits are superposed in the plots, and the corresponding equations are shown in each panel. Colors are blue for B_r , red for B_t , and green for B_n .

Kolmogorovian cascade and the lower frequencies. This behavior has been observed elsewhere in space plasma turbulence (Bruno and Carbone, 2013). The PSD is noted to be higher and steeper for the B_t - and B_n -components than for the B_r -component both for the high-frequency and the low-frequency portions of the spectrum. This means that there is larger spectral power along the entire frequency range for the transverse components of the IMF, indicating larger fluctuations in that direction. The PSDs for the B_t (1.71)- and B_n (1.76)-components are more steeper than for the B_r -component (1.63–1.67). For the low-frequency range, the power indices for the B_r -, B_t -, and B_n -components are close to -1.0 . This is consistent with the results of Bruno and Carbone (2013).

The B_r - and B_n -components have higher power indices in the low frequency range in SCM_{22–23} (Intervals 1 and 2) than in SCM_{23–24} (Intervals 3 and 4). However, the B_t -component power index seems to be dependent on the IMF polarity. It is higher during the Intervals 2 (1995) and 3 (2007), when IMF B_r is positive, than during the Intervals 1 (1994)

and 4 (2008), when B_r is negative. For the high-frequency range that follows Kolmogorov power law, there is no difference between the two solar minima.

4. Summary and Discussions

We presented a comparative study on the solar wind HSS Alfvénic fluctuations during four intervals of high heliospheric latitude (polar) passes of the *Ulysses* spacecraft. These intervals occurred during 1994–1995 and 2007–2008, corresponding to the solar cycle minimum between Cycles 22 and 23 (SCM_{22–23}) and between Cycles 23 and 24 (SCM_{23–24}), respectively. Both southern and northern solar hemispheres were explored by *Ulysses*. The major results are summarized below.

- i) The solar-wind plasma density [N_p] and the IMF magnitude [B_0] were reduced in SCM_{23–24}, if compared to SCM_{22–23}, by $\approx 20\text{--}30\%$. The SCM_{22–23} to SCM_{23–24} reduction in the solar-wind pressure [P_{sw}] was higher ($\approx 40\%$) in the southern hemisphere than in the northern hemisphere ($\approx 20\%$).
- ii) N_p and B_0 were found to be higher in the southern hemisphere by $\approx 3\text{--}6\%$ and $\approx 8\text{--}20\%$, respectively, than in the northern hemisphere.
- iii) The IMF transverse-component variances were $\approx 30\text{--}40\%$ smaller during SCM_{23–24} than during SCM_{22–23}. The reduction in the radial component was $\approx 20\%$.
- iv) The transverse components of the solar-wind velocity and IMF exhibited higher correlation compared to the correlation between their radial components. The correlation coefficient changed sign according to the IMF (B_r) polarity sign, indicating Alfvén waves propagating outward from the Sun.
- v) In general, the correlation between the plasma velocity and IMF components, an indicative of Alfvénicity, was found to be higher during SCM_{22–23} than during SCM_{23–24}.
- vi) The HSS IMF-components had a large range of periodicities, from ≈ 8 hours to ≈ 10 days. While the HSS Alfvén waves had their peak occurrence at periods from 1 to 5 days in both solar minima, the wavelet spectral power density was higher during SCM_{22–23} than during SCM_{23–24}.
- vii) Kurtosis analysis revealed a sub-Gaussian IMF variation during the HSS intervals for the transverse IMF-components and a near-Gaussian variation for the radial-component.
- viii) Fourier power spectrum showed a spectral break around 10^{-4} Hz for all components and intervals. The high-frequency range of the spectrum follows a -1.7 or $-5/3$ power law dependence, which corresponds to the Kolmogorov spectrum. On the other hand, the low-frequency range has a power index law close to -1.0 . This low-frequency index was slightly higher during SCM_{22–23} (-0.65 to -0.87) than during SCM_{23–24} (-0.49 to -0.78). No clear difference was found in the power law index for the high-frequency range. The spectral power was also noted to be always higher for the IMF B_t - and B_n -components than for the B_r -component.

Previous studies (e.g. Smith et al., 1995; Tsurutani et al., 1996) have shown the presence of Alfvén waves in the 1994 and 1995 *Ulysses* polar passes. For a short (24 hours) interval in 1994, Tsurutani et al. (1996) have shown high correlation between the plasma velocity- and IMF-components, with higher correlation for the T- and N-components, which agrees with the present results (Figure 4, Table 3). Smith et al. (1995) have performed the correlation analysis for a 1994 period (different from the one studied here). They reported a high correlation between B_n and V_n . Further, the correlation coefficient calculated for 26-day running averaged intervals from 1992 to 1995 showed a clear increase from the ecliptic plane to the

high heliolatitudes and a reversal from positive in 1994 to negative in 1995. The latter result agrees with our findings.

In the present work, the major wavelet spectral power density was found in the range of 1.5–3 days and around 6 days. Some periods shorter than 1 day were also found in the wavelet spectra. The periods in the range of a few hours, ≈ 1 –10 hours, have been reported in the solar-wind Alfvénic intervals (e.g. Smith et al., 1995; Souza et al., 2016). Smith et al. (1995) found a large coherence between B_n and V_n for a period of ≈ 10 hours. Alfvén waves were found to have periods significantly longer than 1 hour. Bruno, Bavassano, and Villante (1985), using *Helios 1* and 2 observations, reported Alfvén waves with periods longer than 10 hours and up to 15 hours. There were also very short (few hours) periods noted in the wavelet spectrum, but their spectral power is much lower than that of longer periods. Overall, periods shorter than 3 days were sporadic or local, while periods longer than 3 days tended to be more quasi-continuously persistent along the intervals.

Wavelet analysis was also performed using the solar-wind velocity components (not shown to save space). The major periods were found to be in the range of ≈ 2 –17 days, with higher spectral power for the longer periods. A period of ≈ 3 days was observed in the velocity components during the four intervals. This is consistent with the similar period observed in IMF components (Denton and Borovsky, 2012). Verma and Joshi (1994) and Tulasi, Liu, and Su (2010) observed periods of ≈ 9 days in HSS during 1994 and 2007. The 9-day periodicity, that is, $\approx 1/3$ of the solar rotation (coronal hole) period (≈ 27 days), is suggested to be associated with the energy build-up time taken by the coronal holes to produce HSSs.

In general, we found longer Alfvén wave periods at high polar regions than near the ecliptic plane (reported in previous works, e.g., Smith et al., 1995; Souza et al., 2016). A possible explanation, as given by (Bruno and Carbone, 2013), is that at high heliographic latitudes, there is no dynamic interaction between solar-wind streams with different speeds. This lack of strong solar-wind speed shears would enable the occurrence of long-duration Alfvénic fluctuations of extremely low frequency for longer heliocentric distances as observed here at 2 AU. An alternative explanation is the parametric decay instability of Alfvén waves that induces the inverse cascade (Chandran, 2018; Reville, Tenerani, and Velli, 2018; Shoda, Yokoyama, and Suzuki, 2018).

For instance, it was shown theoretically that the f^{-1} power law of solar-wind fast streams in the frequency range higher than $> 3.10^{-4}$ Hz, at distances lower than 0.3 AU, might be locally produced by the parametric decay instability (Chandran, 2018). Further, simulation results showed that high-frequency ($> 10^{-3}$ Hz) Alfvén waves are subjected to a parametric decay instability. This indicates that the solar wind has a frequency filtering effect on the Alfvén waves, and as a result, the medium frequency wave is likely to permeate the interplanetary medium. This is a possible reason for the hour-scale waves observed in the solar wind (Shoda, Yokoyama, and Suzuki, 2018). Finally, Reville, Tenerani, and Velli (2018) using numerical simulations showed that a parametric instability enables an inverse energy cascade by exciting several-hour-long periods of the Alfvénic fluctuations together with strong density fluctuations in the solar wind.

From the power spectrum analyses, the transverse IMF-components are found to have steeper spectra than the radial component. Tsurutani et al. (1996) explored (high-resolution Ulysses magnetic field data) HSSs at a heliocentric distance of 2.4 AU, for a 2-day interval in 1994. At the heliolatitude of -79° , the transverse IMF-components and B_0 are found to exhibit a power law dependence of -1.6 to -1.7 . Over the south pole, HSSs are found to have large-amplitude ($dB/B \approx 1$ –2) nonlinear Alfvén waves. Corresponding power spectrum in the range 10^{-5} to 10^{-2} Hz had a power law index of -1.6 for the transverse component,

and -1.2 for the compressional components. Smith et al. (1995) presented the solar-wind power spectrum analysis for over a year in 1993–1994 covering larger variations in heliocentric distance and latitude. They noted that both IMF magnitude and transverse component spectra have a slope of -1.0 over a much wider range of frequency, with a flat distribution at a period of 10 days. Overall, the solar-wind spectral analysis results obtained here are consistent with previous results. Typically the fast solar wind shows a -1.0 power law index scaling at low frequencies. This is usual for the large-scale energy containing eddies (D'Amicis, Matteini, and Bruno, 2019).

In a work studying the power spectrum of *Helios* 2 during fast streams, Bruno et al. (2009) found that the fast stream power spectrum is characterized by two spectral laws: a power index of -1.0 in lower frequencies and a Kolmogorov near $-5/3$ law at high frequencies. Further, it was found that these two regimes were separated by a spectral break. Recently, the *Parker Solar Probe* spacecraft observations showed the radial evolution of the solar-wind turbulence from 0.17 AU to 1 AU away from the Sun. The IMF spectrum showed a spectral break with a power law of -1.0 at lower frequencies, and $-3/2$ at higher frequencies (10^{-2} to 10^{-1} Hz), similar to the profile observed in the present work (Chen et al., 2020). This high-frequency (inertial range) index varies with heliocentric distance.

In a study using the *Ulysses* observations of the solar-wind velocity, Roberts (2007) derived the spectral index law for several heliocentric distances and latitudes. They have found that, near 2 AU, at high latitudes the power law index is smaller (≈ -1.0 to -1.2). The smaller values are associated with the highly Alfvénic fast polar winds.

The kurtosis values < 3 for the B_t - and B_n -components found in this work indicate dominating low-frequency Alfvén waves with a sub-Gaussian behavior, absence of extreme events and reduced intermittence. This further indicates quasi-steady condition of the HSSs embedded with pure Alfvén waves. According to Mouri et al. (2002), the sub-Gaussian behavior is due to quasi-periodic waves that gave finite amplitude for the fluctuations and do not lead to fully developed turbulence. For comparison, it can be noted that Echer and Bolzan (2016) reported kurtosis values close to 3 for the solar wind upstream of the Uranus magnetosphere, while the values are found to be higher for the foreshock solar wind. In the ecliptic plane, Echer, Bolzan, and Franco (2020) studied the kurtosis evolution using *Ulysses* data and found much higher values, up to 50 for B_0 . It was most likely due to the presence of CIRs and ICMEs causing large-scale disturbances in the solar wind.

5. Conclusions

In the 2007–2009 solar minimum (SCM_{23–24}), the regions around the solar poles were dominated by one magnetic polarity covering a smaller area than in 1996. The solar wind had weaker magnetic flux and was less unipolar, with consequently weaker polar fields, but with complex coronal structure (de Toma, 2012). As a consequence, there were lower densities and magnetic fields in the polar regions (McComas et al., 2008; Smith and Balogh, 2008). In contrast, the corona and heliosphere remained relatively complex in this minimum (de Toma, 2012). From the results obtained in the present study, it can be concluded that while the Alfvénic activity was present in both minima and its general characteristics did not change substantially (sub-Gaussian behavior, power law index with a spectral break near 10^{-4} Hz with high frequency following a Kolmogorov law of $-5/3$, and low-frequency portion with approximately a -1.0 scaling, similar range of periodicity) from one minimum to the other, their fluctuation amplitudes were more reduced in SCM_{23–24} than in SCM_{22–23}.

This reduced power in the Alfvénic fluctuations can have important consequences in interplanetary space dynamics and in energetic particle propagation through the heliosphere.

Alfvénic turbulence has been known to be the dominant mode of solar-wind fluctuations (Bruno and Carbone, 2013). The fact that Alfvénic fluctuations show similar properties over the two solar minima can be attributed to its characteristics. Further, it has been noted that solar polar Alfvénic turbulence evolves similarly as the turbulence in the ecliptic plane, but at a slower rate because of the absence of the shear effects due to large-scale stream interaction (Bruno and Carbone, 2013). The major difference found between SCM_{23–24} and SCM_{22–23} is a reduction in the amplitude of the Alfvénic fluctuations in SCM_{23–24}. This result could be explained in terms of the overall lower magnetic field and solar-wind pressure during SCM_{23–24} (Tsurutani, Echer, and Gonzalez, 2011). During solar wind intervals embedded with Alfvén waves, it has been observed that Alfvénic amplitudes are very large, reaching the nonlinear regime, with the variation of wave activity being a significant proportion of the total field (Tsurutani et al., 1996). Thus, a lower ambient magnetic field would imply a lower amplitude of the Alfvénic fluctuations. Further, Alfvén waves are considered remnants of the heating processes that occur in the solar corona and propagate out of the Sun, using as medium of propagation the magnetic-field lines and the highly ionized plasma that composes the solar wind (Belcher, Davis Jr., and Smith, 1969). As the origin of Alfvénic fluctuations are HSSs emanating from coronal holes, the lower density and pressure of the solar wind indicate a possible lower energy dissipation in SCM_{23–24}, and therefore less potential energy available for generation or amplification of Alfvénic fluctuations in HSSs. These results could be interpreted as the lower Alfvén wave energy injection in SCM_{23–24}. If the Alfvén waves are less efficiently injected in the corona, then because of the lower heating and acceleration of the solar wind, the solar-wind density and pressure should decrease. The Alfvén wave amplitude should also be smaller. One possible mechanism that causes the smaller amount of the Alfvén wave energy during SCM_{23–24} is the less efficient small-scale flux emergence (Wang, 2020).

It will be of interest in future works to study the small-scale features of HSSs during these two minima, investigating for instance interplanetary directional discontinuities and magnetic decreases as well as the turbulence level in these micro-scales of the solar wind. Also, it would be interesting to compare the HSS properties in other regions of the heliosphere, such as near the ecliptic plane and at 1 AU region, during these two solar cycle minima.

Acknowledgments E. Echer would like to thank Brazilian agencies for research grants: CNPq (contract no. PQ-302583/2015-7, PQ-301883/2019-0) and FAPESP (2018/21657-1). The work of R. Hajra is funded by the Science and Engineering Research Board (SERB, grant no. SB/S2/RJN-080/2018), a statutory body of the Department of Science and Technology (DST), Government of India through the Ramanujan Fellowship. The work of A. M. S. Franco is funded by the Brazilian CNPq agency (project no. PQ-300969/2020-1, PQ-301542/2021-0, PQ-300160/2021-6). The work of M. J. A. Bolzan was supported by CNPq agency (contract no. PQ-302330/2015-1, PQ-305692/2018-6) and FAPEG agency (contract no. 2012.1026.7000905). We thank the Brazilian Ministry of Science, Technology and Innovation and the Brazilian Space Agency as well.

Author contributions EE conceived and designed the analysis, and drafted the paper. Analyses were partially performed by EE, AMSF, ECJ and MJAB. RH contributed in interpreting the results. All authors took part in preparing the draft, and approved the final version of the paper.

Data Availability The *Ulysses* data analyzed in this work are collected from NASA's COHOWeb (omniweb.gsfc.nasa.gov/coho/).

Declarations

Competing interests The authors declare no competing interests.

References

- Alfvén, H.: 1942, Existence of electromagnetic-hydrodynamic waves. *Nature* **150**, 405. [DOI](#).
- Balogh, A., Erdős, G.: 2013, The heliospheric magnetic field. *Space Sci. Rev.* **176**, 177. [DOI](#).
- Balogh, A., Beek, T.J., Forsyth, R.J., Hedgecock, P.C., Marquedant, R.J., Smith, E.J., Southwood, D.J., Tsurutani, B.T.: 1992, The magnetic field investigation on the Ulysses mission: instrumentation and preliminary scientific results. *Astron. Astrophys. Suppl. Ser.* **92**, 221.
- Balogh, A., Forsyth, R.J., Lucek, E.A., Horbury, T.S., Smith, E.J.: 1999, Heliospheric magnetic field polarity inversions at high heliographic latitudes. *Geophys. Res. Lett.* **26**, 631. [DOI](#).
- Bame, S.J., McComas, D.J., Barraclough, B.L., Phillips, J.L., Sofaly, K.J., Chavez, J.C., Goldstein, B.E., Sakurai, R.K.: 1992, The Ulysses solar wind plasma experiment. *Astron. Astrophys. Suppl. Ser.* **92**, 227.
- Belcher, J.W., Davis Jr., L.: 1971, Large-amplitude Alfvén waves in the interplanetary medium. *2. J. Geophys. Res.* **76**, 3534. [DOI](#).
- Belcher, J.W., Davis Jr., L., Smith, E.J.: 1969, Large-amplitude Alfvén waves in the interplanetary medium: Mariner 5. *J. Geophys. Res.* **74**, 2302. [DOI](#).
- Bittencourt, J.A.: 2010, *Fundamentals of Plasma Physics*, Springer, Berlin, 679. ISBN: 9781441919304.
- Bolzan, M.J.A., Echer, E.: 2014, A multifractal approach applied to the magnetic field turbulence in Jupiter's magnetosheath. *Planet. Space Sci.* **91**, 77.
- Bracewell, R.N.: 2014, *The Fourier Transform and Its Applications*, 3rd edn. McGraw-Hill Science/Engineering/Math, New York, USA. ISBN13 978-0073039381.
- Bruno, R., Bavassano, B., Villante, U.: 1985, Evidence for long period Alfvén waves in the inner solar system. *J. Geophys. Res.* **90**, 4373. [DOI](#).
- Bruno, R., Carbone, V.: 2013, The solar wind as a turbulence laboratory. *Living Rev. Solar Phys.* **10**, 2. [DOI](#).
- Bruno, R., Carbone, V., Vörös, Z., D'Amicis, R., Bavassano, B., Cattaneo, M.B., Mura, A., Milillo, A., Orsini, S., Veltri, P., Sorriso-Valvo, L., Zhang, T., Biernat, H., Rucker, H., Baumjohann, W., Jankovičová, D., Kovács, P.: 2009, Coordinated study on solar wind turbulence during the Venus-express, ACE and Ulysses alignment of August 2007. *Earth Moon Planets* **104**, 101. [DOI](#).
- Chandran, B.D.G.: 2018, Parametric instability, inverse cascade and the 1/f range of solar-wind turbulence. *J. Plasma Phys.* **84**, 1. [DOI](#).
- Chen, C.H.K., Bale, S.D., Bonnell, J.W., Borovikov, D., Bowen, T.A., Burgess, D., Case, A.W., Chandran, B.D.G., Dudok de Wit, T., Goetz, K., Harvey, P.R., Kasper, J.C., Klein, K.G., Korreck, K.E., Larson, D., Livi, R., MacDowall, R.J., Malaspina, D.M., Mallet, A., McManus, M.D., Moncuquet, M., Pulupa, M., Stevens, M.L., Whittlesey, P.: 2020, The evolution and role of solar wind turbulence in the inner heliosphere. *Astrophys. J. Suppl. Ser.* **246**, 53. [DOI](#).
- Cranmer, S.R.: 2009, Coronal holes. *Living Rev. Solar Phys.* **6**, 3. [DOI](#).
- D'Amicis, R., Matteini, L., Bruno, R.: 2019, On the slow solar wind with high Alfvénicity: from composition and microphysics to spectral properties. *Mon. Not. Roy. Astron. Soc.* **483**, 4665. [DOI](#).
- Davis, J.C.: 2002, *Statistics and Data Analysis in Geology*, Wiley, New York. ISBN 9780471172758.
- de Toma, G.: 2012, Polar magnetic fields and coronal holes during the recent solar minima. In: *Proceedings IAU Symp. No. 286*, 1.
- Denton, M.H., Borovsky, J.E.: 2012, Magnetosphere response to high-speed solar wind streams: a comparison of weak and strong driving and the importance of extended periods of fast solar wind. *J. Geophys. Res.* **117**, A00L05. [DOI](#).
- Dunzlaff, P., Heber, B., Kopp, A., Rother, O., Muller-Mellin, R., Klassen, A., Gomez-Herrero, R., Wimmer-Schweingruber, R.: 2008, Observations of recurrent cosmic ray decreases during solar cycles 22 and 23. *Ann. Geophys.* **26**, 3127. [DOI](#).
- Ebert, R.W., McComas, D.J., Elliott, H.A., Forsyth, R.J., Gosling, J.T.: 2009, Bulk properties of the slow and fast solar wind and interplanetary coronal mass ejections measured by Ulysses: three polar orbits of observations. *J. Geophys. Res.* **114**, A01109. [DOI](#).
- Echer, E., Bolzan, M.J.A.: 2016, A comparative study of solar wind and foreshock turbulence near Uranus orbit. *Planet. Space Sci.* **120**, 70. [DOI](#).
- Echer, E., Bolzan, M.J.A., Franco, A.M.S.: 2020, Statistical analysis of solar wind parameter variation with heliospheric distance: Ulysses observations in the ecliptic plane. *Adv. Space Res.* **65**, 2846. [DOI](#).
- Franco, A.M.S., Franz, M., Echer, E., Bolzan, M.J.A.: 2020, Wavelet analysis of low frequency plasma oscillations in the magnetosheath of Mars. *Adv. Space Res.* **65**, 2090. [DOI](#).
- Franco, A.M.S., Hajra, R., Echer, E., Bolzan, M.J.A.: 2021, Seasonal features of geomagnetic activity: a study on the solar activity dependence. *Ann. Geophys.* **39**, 929. [DOI](#).
- Franco, A.M.S., Echer, E., Bolzan, M.J.A., Franz, M.: 2022, Study of fluctuations in the Martian magnetosheath using a kurtosis technique: Mars Express observations. *Earth Planet. Phys.* **6**, 28. [DOI](#).

- Gloeckler, G., Allegrini, F., Elliott, H.A., McComas, D.J., Schwadron, N.A., Geiss, J., von Steiger, R., Jones, G.H.: 2004, Cometary ions trapped in a coronal mass ejection. *Astrophys. J.* **604**, L121. [DOI](#).
- Gosling, J.T., Bame, S.J., McComas, D.J., Phillips, J.L., Pizzo, V.J., Goldstein, B.E., Neugebauer, M.: 1993, Latitudinal variation of solar wind corotating stream interaction regions: Ulysses. *Geophys. Res. Lett.* **20**, 2789. [DOI](#).
- Hajra, R.: 2021, Weakest solar cycle of the space age: a study on solar wind–magnetosphere energy coupling and geomagnetic activity. *Solar Phys.* **296**, 33. [DOI](#).
- Hajra, R., Franco, A.M.S., Echer, E., Bolzan, M.J.A.: 2021, Long-term variations of the geomagnetic activity: a comparison between the strong and weak solar activity cycles and implications for the space climate. *J. Geophys. Res.* **126**, e2020JA028695. [DOI](#).
- Hathaway, D.H.: 2010, The solar cycle. *Living Rev. Solar Phys.* **7**, 1. [DOI](#).
- Jimenez, J.: 1998, Turbulent velocity fluctuations need not be Gaussian. *J. Fluid Mech.* **376**, 139. [DOI](#).
- Jones, G.H., Balogh, A., Horbury, T.S.: 2000, Identification of comet Hyakutake's extremely long ion tail from magnetic field signatures. *Nature* **404**, 574. [DOI](#).
- Krieger, A.S., Timothy, A.F., Roelof, E.C.: 1973, A coronal hole and its identification as the source of a high velocity solar wind stream. *Solar Phys.* **29**, 505. [DOI](#).
- McComas, D.J., Barraclough, B.L., Funsten, H.O., Gosling, J.T., Santiago-Muñoz, E., Skoug, R.M., Goldstein, B.E., Neugebauer, M., Riley, P., Balogh, A.: 2000, Solar wind observations over Ulysses' first full polar orbit. *J. Geophys. Res.* **105**, 10419. [DOI](#).
- McComas, D.J., Elliott, H.A., Gosling, J.T., Reisenfeld, D.B., Skoug, R.M., Goldstein, B.E., Neugebauer, M., Balogh, A.: 2002, Ulysses' second fast-latitude scan: complexity near solar maximum and the reformation of polar coronal holes. *Geophys. Res. Lett.* **29**, 4. [DOI](#).
- McComas, D.J., Elliott, H.A., Schwadron, N.A., Gosling, J.T., Skoug, R.M., Goldstein, B.E.: 2003, The three-dimensional solar wind around solar maximum. *Geophys. Res. Lett.* **30**, 1517. [DOI](#).
- McComas, D.J., Ebert, R.W., Elliott, H.A., Goldstein, B.E., Gosling, J.T., Schwadron, N.A., Skoug, R.M.: 2008, Weaker solar wind from the polar coronal holes and the whole Sun. *Geophys. Res. Lett.* **35**, L18103. [DOI](#).
- Mouri, H., Takaoka, M., Hori, A., Kawashima, Y.: 2002, Probability density function of turbulent velocity fluctuations. *Phys. Rev. E* **65**, 056304. [DOI](#).
- Neugebauer, M.: 1999, The three-dimensional solar wind at solar activity minimum. *Rev. Geophys.* **37**, 107. [DOI](#).
- Neugebauer, M., Liewer, P.C., Smith, E.J., Skoug, R.M., Zurbuchen, T.H.: 2002, Sources of the solar wind at solar activity maximum. *J. Geophys. Res.* **107**, SSH 13. [DOI](#).
- Neugebauer, M., Gloeckler, G., Gosling, J.T., Rees, A., Skoug, R., Goldstein, B.E., Armstrong, T.P., Combi, M.R., Mäkinen, T., McComas, D.J., von Steiger, R., Zurbuchen, T.H., Smith, E.J., Geiss, J., Lanzerotti, L.J.: 2007, Encounter of the Ulysses spacecraft with the ion tail of comet McNaught. *Astrophys. J.* **604**, L121. [DOI](#).
- Phillips, J.L., Bame, S.J., Barnes, A., Barraclough, B.L., Feldman, W.C., Goldstein, B.E., Gosling, J.T., Hoogeveen, G.W., McComas, D.J., Neugebauer, M., Suess, S.T.: 1995, Ulysses solar wind plasma observations from pole to pole. *Geophys. Res. Lett.* **22**, 3301. [DOI](#).
- Priest, E.R.: 1995, In: Kivelson, M.G., Russell, C.R. (eds.) *The Sun and Its Magnetohydrodynamics*, Cambridge University Press, Cambridge, 58.
- Reville, V., Tenerani, A., Velli, M.: 2018, Parametric decay and the origin of the low-frequency Alfvénic spectrum of the solar wind. *Astrophys. J.* **866**, 38. [DOI](#).
- Richardson, I.G.: 2014, Identification of interplanetary coronal mass ejections at Ulysses using multiple solar wind signatures. *Solar Phys.* **289**, 3843. [DOI](#).
- Roberts, D.A.: 2007, The evolution of the spectrum of velocity fluctuations in the solar wind. *Eos Trans. AGU* **88**, SH31B.
- Schrijver, C.J., Liu, Y.: 2008, The global solar magnetic field through a full sunspot cycle: observations and model results. *Solar Phys.* **252**, 19. [DOI](#).
- Schwenn, R.: 2006, Space weather the solar perspective. *Living Rev. Solar Phys.* **3**, 2. [DOI](#).
- Sheeley, N.R., Harvey, J.W., Feldman, W.C.: 1976, Coronal holes, solar wind streams, and recurrent geomagnetic disturbances: 1973–1976. *Solar Phys.* **49**, 271. [DOI](#).
- Shoda, M., Yokoyama, T., Suzuki, T.K.: 2018, Frequency-dependent Alfvén-wave propagation in the solar wind onset and suppression of parametric decay instability. *Astrophys. J.* **860**, 17. [DOI](#).
- Smith, E.J., Balogh, A.: 2008, Decrease in heliospheric magnetic flux in this solar minimum: recent Ulysses magnetic field observations. *Geophys. Res. Lett.* **35**, L22103. [DOI](#).
- Smith, E.J., Wenzel, K.P., Page, D.E.: 1992, Ulysses at Jupiter: an overview of the encounter science. *Science* **257**, 1503. [DOI](#).
- Smith, E.J., Wolfe, J.H.: 1976, Observations of interaction regions and corotating shocks between one and five AU: Pioneers 10 and 11. *Geophys. Res. Lett.* **3**, 137. [DOI](#).

- Smith, E.J., Balogh, A., Neugebauer, M., McComas, D.: 1995, Ulysses observations of Alfvén waves in the southern and northern solar hemispheres. *Geophys. Res. Lett.* **22**, 3381. [DOI](#).
- Smith, E.J., Balogh, A., Forsyth, R.J., McComas, D.J.: 2001, Ulysses in the south polar cap at solar maximum: heliospheric magnetic field. *Geophys. Res. Lett.* **28**, 4159. [DOI](#).
- Souza, A.M., Echer, E., Bolzan, M.J.A., Hajra, R.: 2016, A study on the main periodicities in interplanetary magnetic field Bz component and geomagnetic AE index during HILDCAA events using wavelet analysis. *J. Atmos. Solar-Terr. Phys.* **149**, 81. [DOI](#).
- Torrence, C., Compo, G.P.: 1998, A practical guide to wavelet analysis. *Bull. Am. Meteorol. Soc.* **79**, 61.
- Tsurutani, B.T., Echer, E., Gonzalez, W.D.: 2011, The solar and interplanetary causes of the recent minimum in geomagnetic activity(MGA23): a combination of midlatitude coronal holes, low IMF Bz variances, low solar wind speeds and low solar magnetic fields. *Ann. Geophys.* **29**, 839. [DOI](#).
- Tsurutani, B.T., Ho, C.M., Arballo, J.K., Smith, E.J., Goldstein, B.E., Neugebauer, M., Balogh, A., Feldman, W.C.: 1996, Interplanetary discontinuities and Alfvén waves at high heliographic latitudes: Ulysses. *J. Geophys. Res.* **101**, 11027. [DOI](#).
- Tulasi, R.S., Liu, C.H., Su, S.-Y.: 2010, Periodic solar wind forcing due to recurrent coronal holes during 1996–2009 and its impact on Earth's geomagnetic and ionospheric properties during the extreme solar minimum. *J. Geophys. Res.* **115**, A12340. [DOI](#).
- Verma, V.K., Joshi, G.C.: 1994, On the occurrence rate of high speed solar wind events. *Solar Phys.* **155**, 401. [DOI](#).
- Virtanen, I.I., Mursula, K.: 2010, Asymmetry of solar polar fields and the southward shift of HCS observed by Ulysses. *J. Geophys. Res.* **115**, A09110. [DOI](#).
- Wang, Y.M.: 2020, Small scale emergence, coronal hole heatin and flux expansion a hybrid solar wind model. *Astrophys. J.* **904**, 199. [DOI](#).
- Wang, Y.-M., Sheeley, N.R. Jr.: 2006, Sources of the solar wind at Ulysses during 1990–2006. *Astrophys. J.* **653**, 708. [DOI](#).
- Zhang, M., McKibben, R.B., Lopate, C., Jokipii, J.R., Giacalone, J., Kallenrode, M.-B., Rassoul, H.K.: 2003, Ulysses observations of solar energetic particles from the 14 July 2000 event at high heliographic latitudes. *J. Geophys. Res.* **108**, 1154. [DOI](#).

Publisher's Note Springer Nature remains neutral with regard to jurisdictional claims in published maps and institutional affiliations.

Springer Nature or its licensor (e.g. a society or other partner) holds exclusive rights to this article under a publishing agreement with the author(s) or other rightsholder(s); author self-archiving of the accepted manuscript version of this article is solely governed by the terms of such publishing agreement and applicable law.